

Something more than graphene – futuristic two-dimensional nanomaterials

Inderdeep Singh Bhatia* and Deep Kamal Kaur Randhawa

Department of Electronics and Communication Engineering, Guru Nanak Dev University, Regional Campus, Jalandhar 144 007, India

The race to scale down electronic circuits has resulted in the novel two-dimensional (2D) materials. Graphene, after its discovery in 2004, topped the list on account of its superior electronic, optical, mechanical and transport properties. Since, graphene possesses zero band gap, it could not be used in digital circuits; so other potential 2D materials have been studied. Materials like transition metal dichalcogenides (TMDs), 2D oxides, hexagonal boron nitride and 2D Xenos (silicene, borophene, stanene, phosphorene and borophene) belong to the plethora of materials following the discovery of graphene. They apparently show potential in quantum computing and superfast electronics. They display ballistic transport and relativistic properties due to the mass-less fermions. Quantum spin Hall effect too is observed along with quantum Hall effect in many of them, which advocates their use in spintronics. Owing to these superior properties, they appear to be promising candidates for a paradigm shift from microelectronics to nanoelectronics. The 2D structural analogues of graphene, i.e. silicene, borophene, stanene, phosphorene and germanene are fast emerging alternative 2D materials compared to 2D oxides and TMDs, since they have a better degree of integration with the existing silicon-based technology. This article surveys the emerging 2D materials which hold promise in the future.

Keywords: Two-dimensional materials, nanoelectronics, quantum computing, spintronics, Xenos.

IN order to determine the characteristics of two-dimensional (2D) materials, there have been several studies on different potential materials and their 2D structures. The existence of Dirac fermions, quantum Hall effect (QHE), large carrier mobility, mass-less behaviour of charge carriers and the assurance of minimum current conduction at even zero free-carrier concentration in graphene has initiated studies to find potential materials for further use in very large-scale integration (VLSI), optoelectronics, memory devices and sensors¹. This led to the exploration of a pool of 2D materials, including transition metal chalcogenides (TMDs), hexagonal boron nitrides (h-BN), 2D oxides and 2D Xenos (Figure 1)²⁻⁴. Even

though a substantial amount of knowledge regarding various properties of these 2D materials has been gained, they could not perform better than graphene in ballistic transport-based applications due to the high Fermi velocity in graphene^{1,5}. This is because of the difference in density of states of charge carriers and different arrangement of constituent atoms of these materials at the nano level compared to graphene⁶.

Figure 2 shows the evolution of different 2D materials versus their band gap range.

Basically 2D materials have a thickness of few atoms or less. Due to the weak interlayer coupling forces they can be split down into independent free layers. The interaction criteria of the applied excitation energy with the outermost shell electrons, contribute to their vivid

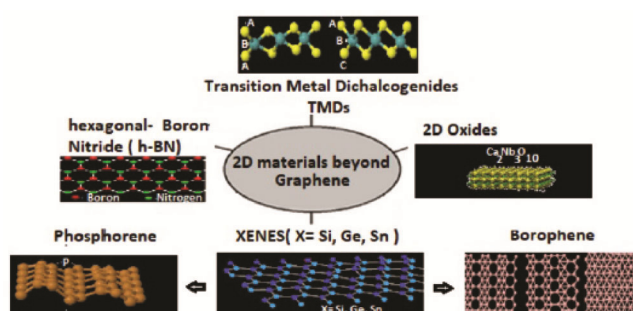


Figure 1. Two-dimensional (2D) materials beyond graphene.

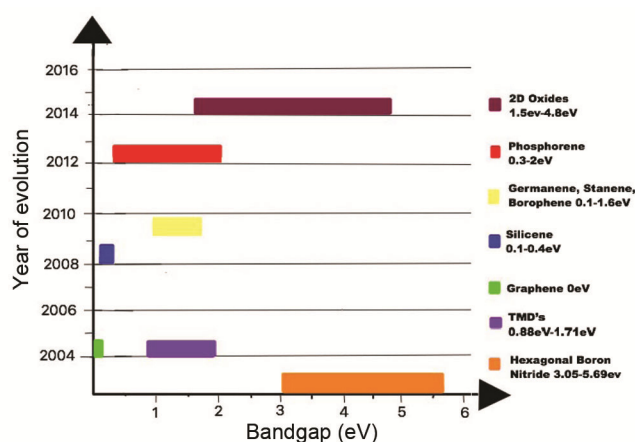


Figure 2. Band gap versus year of evolution for different 2D materials.

*For correspondence. (e-mail: inder.singh1002@gmail.com)

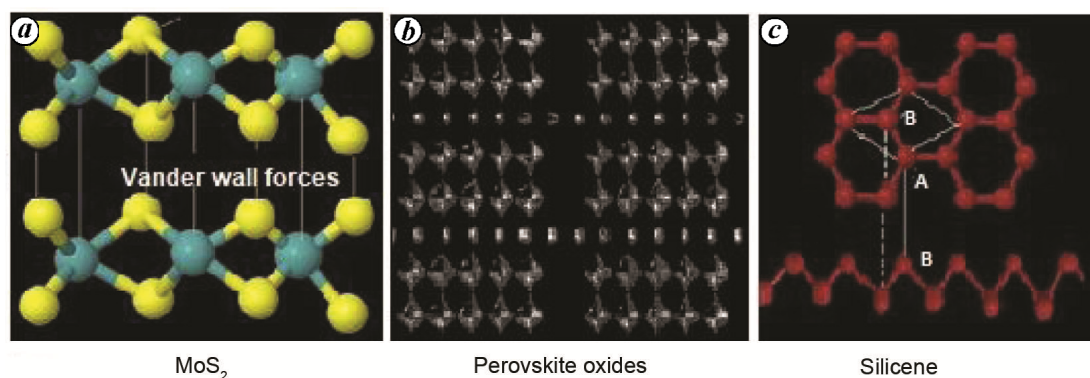


Figure 3. Classification of 2D materials. *a*, van der Waals solids. *b*, Layered ionic solids (reprinted with permission from Ozawa *et al.*¹⁹; ©2019 by the American Physical Society). *c*, Surface-assisted non-layered solids (reprinted with permission from Ni *et al.*¹¹³; ©2019 by the American Physical Society).

properties⁷. The 2D materials can be found in different structural forms like nano island structures, nanoplates, nanosheets, nanowalls and nanodisks^{8–10}. As majority of our biological processes take place at the nanoscale, this provides scientists models and templates to study 2D materials. At the nanoscale, particle properties, viz. melting point, electrical conductivity, magnetic permeability and chemical reactivity are a function of particle size, which can be tuned further.

There are several questions regarding 2D materials. For example, how 2D materials are unique and what makes them attractive and useful at the nanoscale? Why and how are 2D materials different from bulk materials from which they are derived? Can they be the leading materials to shift from micro to nanoscale? Since 2D materials are just one atom thick, Moore's law could be sustained by a higher degree of chip integration^{1,11,12}. The high mobility, chiral properties of charge carriers and presence of Dirac mass less fermions make them suitable for applications in high-speed electronics¹³. QHE is observed in graphene at room temperature, which shows high electron density of up to 10^{13} cm^{-2} and high invariable mobility μ of up to $10,000 \text{ cm}^2 \text{ V}^{-1} \text{ s}^{-1}$ (ref. 14). Similarly, high switching ratios of the order of 10^9 and driving currents of about $320 \mu\text{A} \mu\text{m}^{-1}$ in field-effect transistors using Ohmic contact in 2D materials could be utilized in future VLSI circuits¹⁵. According to structural forms, 2D materials can be classified into three groups as follows.

(i) Layered van der Waals solids: These are a single layer or multiple thick layers of atoms having crystalline structures connected to each other by strong in-plane ionic or intra-layer covalent bonds and by inter-layer van der Waals forces (40–70 MeV)¹⁶. The weak nature of these bonds facilitates the exfoliation of bulk crystalline materials into nanosheets by different methods of exfoliation¹⁶. These exfoliated sheets are usually few microns laterally and about 1 nm thick¹⁷. TMDs, especially MoS_2 , MoSe_2 and WS_2 are members of this family¹⁷ (Figure 3 *a*).

(ii) Layered ionic solids: These are solids which have charged polyhedrons sandwiched between hydroxyl or halide layers due to strong electrostatic forces¹⁸. Single or few layers thick ionic solids can be easily converted into independent, stable, single-layered sheets exfoliated by treatment with different ions¹⁷. Perovskite oxides like $\text{La}_{0.90}\text{Eu}_{0.05}\text{Nb}_2\text{O}_7$ belong to this family¹⁹ (Figure 3 *b*).

(iii) Surface assisted non-layered solids: These belong to the class of one-atom thick, multiple-layered solids which are grown on an ordered substrate using artificial methods like chemical vapour deposition (CVD)^{18,20,21}. The members of this family need a surface for growth, as under ambient conditions they are unstable in nature. Silicene is a perfect example for it (Figure 3 *c*). Si atoms with hexagonal structure depicting low buckling factor have been grown on silver substrate, viz. $\text{Ag}(111)$ ²².

Two-dimensional materials other than graphene

Transition metal dichalcogenides

TMDs are of the type MX_2 , where M refers to transition metals (namely Mo, W, Ti, Zr, Hf, V, Nb, Ta, Tc, Re, Pd, Pt) and X belongs to the Group 16 chalcogen family (S, Se, Te)². These bulk layered materials having strong intra-layer covalent MX bonds are cleaved into single/few layers by the exfoliation process, which depends upon the surface energy (SE). The SE is the energy applied to peel-off a new surface from the crystal surface. The SE of TMDs like MoS_2 and WS_2 (65–75 m per sq. m) is comparable to that of graphene (65–120 m per sq. m) making them potentially cleavable^{23,24}.

Structure of TMDs: Different structural phases exist in TMDs due to the different arrangement of coordination spheres of transition metal atoms. A single-layer TMD can exist as a trigonal prismatic or as an octahedral phase^{19,25}. The trigonal prismatic phase, i.e. 2H phase (or

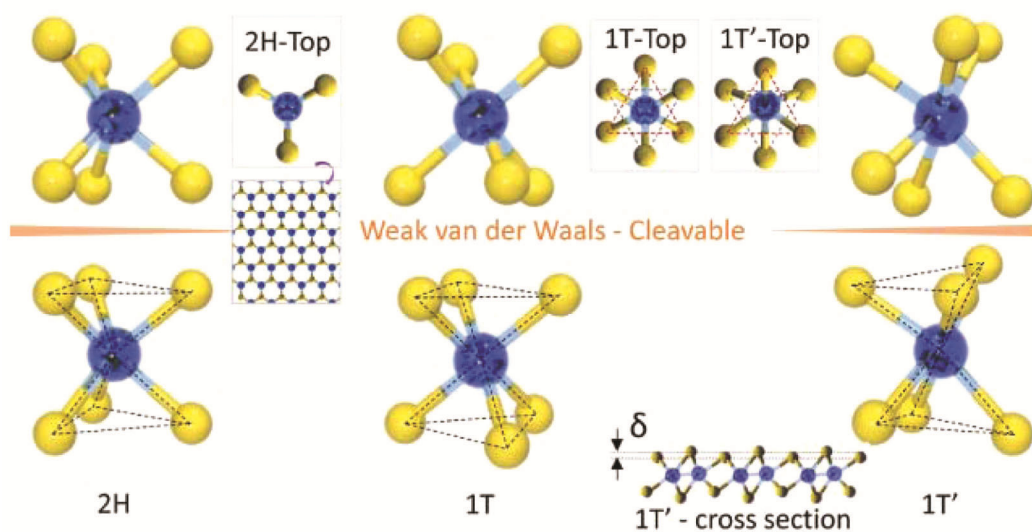


Figure 4. Different structural forms for transition metal dichalcogenides (TMDs) 2H, 1T and 1T'. (Reprinted with permission from Choi *et al.*²⁷.)

1H for a single layer) has a hexagonal symmetry (D_{3h} group). In this geometry, the chalcogen atoms align vertically along the z -axis in case of single layers and the stack in 'ABA' sequence (where A and B represent Group 16 chalcogen and transition metal atoms respectively)²⁶. Tetragonal symmetry (D_{3d}) is present in the octahedral phase, which refers to an octahedral arrangement of the metal atoms. In the octahedral phase (1T phase) one of the chalcogen layers is displaced, thus forming an ABC sequenced stack. The atomic structure of TMD layers is affected by the manner in which the d -orbital are filled¹⁷. Trigonal prismatic (2H) phases are usually seen in the Group 4 (d^0) and Group 6 (d^2) TMDs. Group 5 (d^1) TMDs can have either trigonal prismatic (2H) or octahedral phases (1T), whereas distorted octahedral structure is observed in Group 7 TMDs. Group 10 TMDs (d^6) have an octahedral phase. In addition to the 1T and 1H phases, 1H layers can be stacked in two different ways which impart hexagonal symmetry (2H phase, symmetry D_{4h}) like ABA BAB or rhombohedral symmetry (3R, symmetry C_{3v}) with the ABA CAC BCB stacking sequence²⁷. ABC ABC sequence is seen in the 1T layer²⁷. This diversity in the order of stack formation produces defects and also imparts new characteristics to the material due to breaking of the order of symmetry. Recently, monolayer TMDs in 1T' (or distorted octahedral phase) have also been synthesized in bulk²⁷. It has been observed that phase transition from 1T to 1T' causes band inversion and leads to topological phase transition². Among different polytypes in MX_2 , the most studied and stable form is the 2H phase (band gap > 1 eV). This phase also exhibits strong valley polarization due to inversion symmetry breaking. The 1T phase is however metallic with inversion symmetry. It can be engineered using carrier doping²⁸ and phase patterning²⁹ to form a

metastable phase. Due to electron–phonon interactions², the 1T phase spontaneously transforms to the stable 1T' phase, which also has inversion symmetry. Figure 4 shows the different structural phases of TMDs²⁷.

Synthesis of TMD layers (MoS_2 and WS_2): The synthesis of TMDs can be done by top-down or bottom-up methods. To obtain a single or few layers of TMDs from their bulk, top-down methods are used². Mechanical exfoliation is the prevalent method used to produce the highest quality single-layer MX_2 . However, it is not used for large-scale production due to lesser output. Single-layered MoS_2 can also be obtained using thermal ablation by lasers. Lithium intercalation is used for high yields of TMDs²⁵. The disadvantage of this method is that the product loses its semiconducting properties. In the bottom-up methods, CVD is used to produce a single or few layers of TMDs from their atoms or molecules¹⁷. MoS_2 , WS_2 and other TMDs are widely synthesized using this technique. Figure 5a shows STM image of WS_2 grown on graphene.

Band structure and electronic properties of TMDs: The vivid chemical compositions and structural phases of TMDs account for a broad range of their electronic properties. The band structure of TMDs of group 6 transition metals (Mo, W) with S and Se is discussed here. The 2H polytype of TMDs is thermodynamically stable and is a semiconductor³⁰. Their band gap can be engineered by changing the thickness of their bulk materials to a single monolayer³¹. The band gap of MoS_2 (2H) bulk and monolayer is calculated as 0.88 and 1.71 eV respectively³². MoS_2 , $MoSe_2$, WS_2 and WSe_2 are semiconductors, WTe_2 and $TiSe_2$ behave as semimetals, VSe_2 and NbS_2 exhibit metallic character, while $NbSe_2$ and TaS_2 are

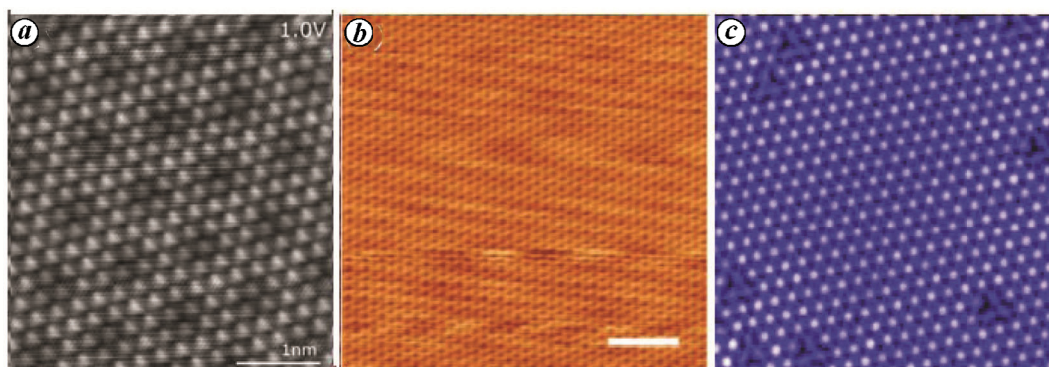


Figure 5. STM images of (a) WS₂ on graphene (reprinted from Kastl *et al.*¹¹⁴), (b) 2D-hBN (reprinted from Haque *et al.*⁴⁸) and (c) LiTi₂O₄ thin film (reprinted from Okada *et al.*⁶²).

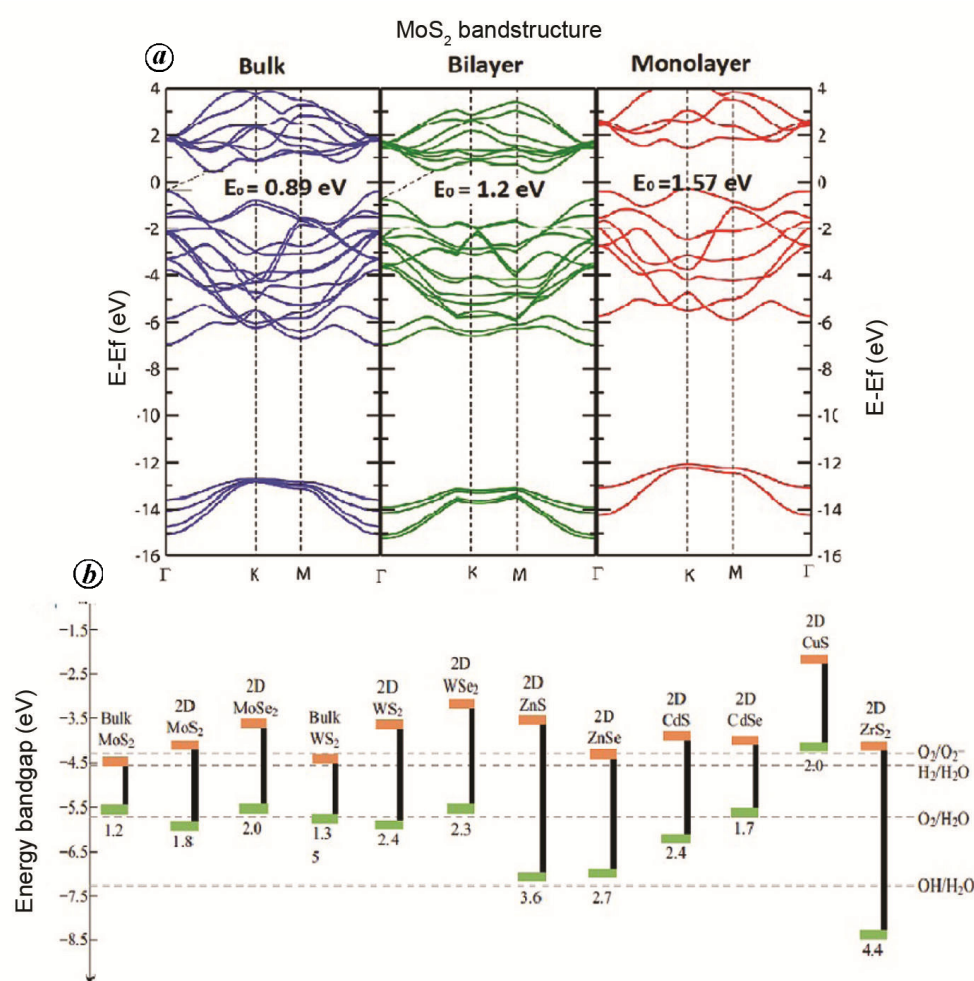


Figure 6. a, Band structure of bulk, bilayer and monolayer MoS₂ (reprinted from Ahmad and Mukherjee³⁴). b, Energy band gap of different 2D TMDs (reprinted from Haque *et al.*¹¹¹).

superconducting. These 2D TMDs show large mobility (~ 200 cm² V⁻¹ s⁻¹) at room temperature, high current switching ratios (1×10^8) and low power dissipation which is comparable to that of graphene³³. Figure 6a shows the band structure of bulk, bilayer and monolayer

MoS₂ while Figure 6b shows the energy band gap of different 2D TMDs.

Optical properties of TMDs: On analysis of the band structure of TMDs, the conduction and valence band

edges are seen to be at two different energy degenerate valleys which lie at the corner of the first Brillouin zone³⁴. The valley polarization process is then used to control the population of electrons in the valleys, thereby using TMDs in valley-based electronics and optoelectronics applications³⁵.

Mechanical properties of TMDs: For the intended use in flexible electronics, the mechanical properties of TMDs must also be known. In an experiment on the stretching and breaking power of mono- and bi-layered MoS₂ the atomic force microscope (AFM) test method was used. The experimental results revealed the in-plane stiffness ($\sim 180 \pm 60$ N/m) and Young's modulus ($\sim 270 \pm 100$ GPa) of a monolayer MoS₂ which is almost equal to that of steel³⁶. It was also observed that the breaking strength of MoS₂ was around 23 GPa, about 11% of its Young's modulus³⁶. This indicated the highly crystalline and defect-free structure which could be used for different strength demanding applications. In a similar analysis WS₂ yielded a Young's modulus of 171 GPa, supporting the use of TMDs in flexible electronics³⁷.

Magnetic properties of TMDs: The spin-spin splitting property makes layered TMDs suitable for spin-based applications, but due to their non-magnetic property such use was hampered. However, recently, a strategy to induce ferromagnetism in non-magnetic MoS₂ has been developed. By integrating the 1T phase of MoS₂ in 2H MoS₂, a Curie temperature of 395 K was achieved³⁸. The intensity of magnetization in 2H-MoS₂ nanosheets at 300 K was enhanced from 0.02 to 0.25 $\mu\text{B}/\text{Mo}$, thereby tuning in the magnetic properties of TMDs³⁸.

Applications of TMDs: Mo and W dichalcogenides with 1–2 eV band gap provide fast digital switching of the order of 10⁸; large carrier mobility (~ 700 cm² V⁻¹ s⁻¹) a large optical absorption ($\sim 10^7$ m⁻¹) and substantial photoluminescence arising from the direct band gap^{39,40}. The monolayer MoS₂ photodetectors show ultra sensitivity with the responsivity ranging from 400 to 680 nm (ref. 41). These results unfold the applications of MoS₂-derived electronic circuits in light sensors and optoelectronic devices. The interplanar stiffness of about 180 N/m and Young's modulus of about 270 GPa, which is equivalent to that of steel, make it useful for flexible electronics⁴⁰.

Two-dimensional hexagonal boron nitride (h-BN): h-BN is a wide band gap semiconductor with a forbidden energy gap of the order of 5.9 eV (ref. 42). It is layered and isostructural to graphite. The monolayer h-BN sheets find use as high-quality dielectric layers in graphene-based devices, as they have a smooth surface due to the absence of charge traps and dangling bonds⁴³. Some studies have shown the high thermal and chemical stabi-

ties of h-BN against corrosion by oxidation thereby suggesting that its thin layer can be used for corrosion inhibiting nano-coatings⁴¹.

Structure of h-BN: h-BN has B and N atoms arranged periodically to form a honeycomb structure (Figure 7a)⁴⁴. The B–N bond is formed through *sp*² hybridization and has a bond length of 1.45 Å (ref. 43). van der Waals forces hold together adjacent h-BN layers and within each subsequent layer, boron and nitrogen atoms form covalent bonds. The interlayer spacing in h-BN (~ 0.333 nm) is comparable to that of graphene (~ 0.335 nm)^{45,46}. The bonding force of h-BN is small in the *c*-direction leading to large spacing between the adjacent layers; so interlayer sliding is easier in this case. When compared to graphene, which is metallic in nature by default, the single-layered h-BN is an insulator and is also known as 'white graphene'⁴⁶.

Synthesis of h-BN: h-BN monolayer is synthesized from its bulk by chemical solution-based methods or mechanical exfoliation⁴³. The drawback of using these methods is that the layer formed is imperfect, which decreases its potential use in various applications. Alternate methods used for synthesis are CVD and physical vapour deposition (PVD)⁴⁷. These methods yield a perfect structure, however, they are time-consuming and the production yield is low. Ultra high vacuum (UHV) technique is thus deployed to form high-quality mono-layered h-BN at low vacuum and low substrate temperature⁴⁵. Figure 5b shows the STM image of 2D h-BN (ref. 48).

Band structure and electronic properties of h-BN: h-BN has a high electrical resistivity of the order of 10¹⁷ and 10⁴ ohm-cm at room temperature and 200°C respectively¹¹. For practical applications of h-BN, doping is the only option. The plasma ion implantation method can be deployed for the same⁴⁹. The dopant atoms combine with h-BN in such a way that they develop semiconducting properties⁵⁰. Density functional theory (DFT) and its first principles show that band gap of h-BN is reduced to 3.05 eV when boron and nitrogen atoms are linked with H-atoms on both sides³. Various studies have been done to examine how the physical properties of h-BN change with adatom adsorption²⁷. Different atoms like Fe, Si, C, Pt, Cu, B and Si were considered for this and it was found that most of them are incompatible in binding to the surface. Figure 7b shows the band structure of bulk h-BN.

Optical properties of h-BN: h-BN nanosheets are optically transparent to 99% of wavelengths in the range of 250–900 nm, whereas a sharp absorption peak is seen in the deep ultraviolet range between 200 and 220 nm (ref. 49). Unlike bulk h-BN (5.2–5.4 eV), the monolayer h-BN has an optical band gap of about 6.07 eV (ref. 51). For multilayer h-BN, it ranges from 5.56 to 5.92 eV (ref. 51).

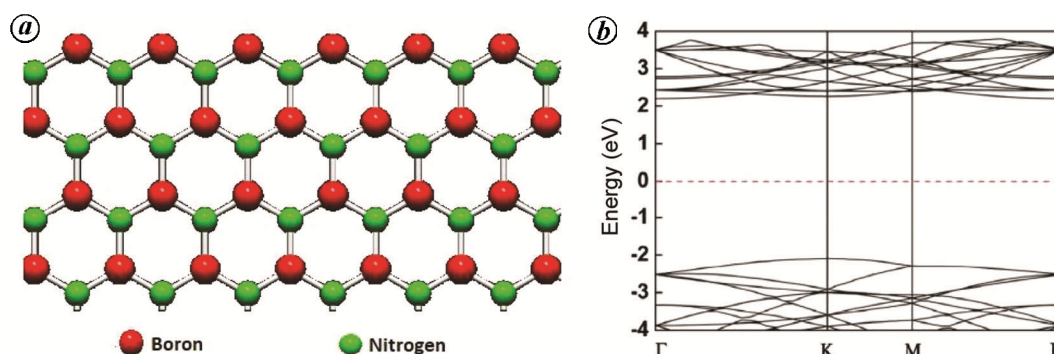


Figure 7. *a*, Hexagonal boron nitride (h-BN) hexagonal graphene-like structure⁴⁴. *b*, Band structure of bulk h-BN (reprinted from Kim *et al.*¹¹⁵).

Due to the direct wide band gap and ultraviolet luminescence property, h-BN nanosheets can be used in ultraviolet lasing, photon emission and photodetectors⁵².

Mechanical properties of h-BN: The in-plane strength of a monolayer h-BN and graphene has been reported in previous studies as 267 and 335 N/m respectively⁵³. Thus, h-BN can be used like reinforcing fillers, e.g. graphene which is used for making polymer composites. Earlier studies have reported that the breaking stress and modulus of h-BN having few nanometer thickness range from 8 to 16 N/m and 220 to 510 N/m respectively⁵⁴. Bulk h-BN due to weak inter-planar forces is used as a lubricant. A study showed that frictional characteristics of the sheets are thickness-dependent⁵⁵; the friction varies inversely with thickness of the sheets.

Magnetic properties of h-BN: h-BN exhibits vivid magnetic properties when it is fused with different atoms around it. It forms anisotropic structures (direction-dependent) with rich magnetic properties when decorated with H- and F-atoms. The h-BN sheets can be made ferromagnetic, anti ferromagnetic or magnetically neutral depending upon the functional groups attached. A study has demonstrated the modulation of magnetic properties through fusion of H- and F-atoms on a h-BN sheet⁵⁶. In semi-decorated structures, H–BN, F–BN and H–NB, the unsaturated N or B atoms have magnetic moments due to the presence of unpaired electrons in $2P_z$ orbital. H–BN and H–NB systems link ferromagnetically and anti-ferromagnetically respectively⁵⁶. However, in the F–BN system, the ferromagnetic and anti-ferromagnetic states show energetic degeneracy⁵⁶.

Applications of h-BN: Due to its wide band gap, 2D h-BN finds several applications in the insulation of devices. Deep UV photodetectors which are commonly used in pollution monitors, protected space communication, information storage and spacecraft applications employ 2D h-BN⁵⁷. Since UV emission from 2D h-BN is found be-

tween 215 and 227 nm, it has become a potential alternative for low-power UV emitters which can be used for various medical purposes. Two-dimensional 2D h-BN also finds applications in gas sensors and can be used in hard environmental conditions⁵⁸. It can also be efficiently used as a gate insulator in 2D field effect transistors that show clear switching behaviour and on/off current ratio greater than 10^6 (ref. 59). The h-BN-based dielectric material can also be used in junction tunnelling devices⁶⁰. Further, tunnelling transport and capability to emit single photon advocates its use in quantum computing based applications⁶⁰.

Two-dimensional layered oxides

The exfoliation of layered compounds exhibits various novel properties in a material due to electron confinement in two-dimensional electron gases (2 DEGs). Similar results have been reported in 2D nanosheets of the transition group metals, rare earth metals and their oxides. In transition metal 2D layered oxides (TMOs), the oxygen being highly electronegative pulls the s -electrons of the transition metal, and as a result the structural, physical and chemical properties are mostly determined by the strongly associated d -electrons. Due to the variety of chemical composition and the easy defect formation, their properties can be tuned in according to the choice of application⁶¹. The physical and chemical properties of two-dimensional TMOs are usually different compared to their bulk counterparts⁶².

Structure and synthesis of 2D layered oxides: Chemical exfoliation of oxide nanosheets with bulky guest ions as intercalation agents leads to a high degree of intermolecular cracking and weakens the forces of attraction between adjacent layers of the sheets. Many internal and external factors like ions between the sheets, electrostatic forces, polarity, surface-tension and dielectric constant are optimized to completely exfoliate the layered compound into single and few layered nanosheets (Figure 8)⁶¹.

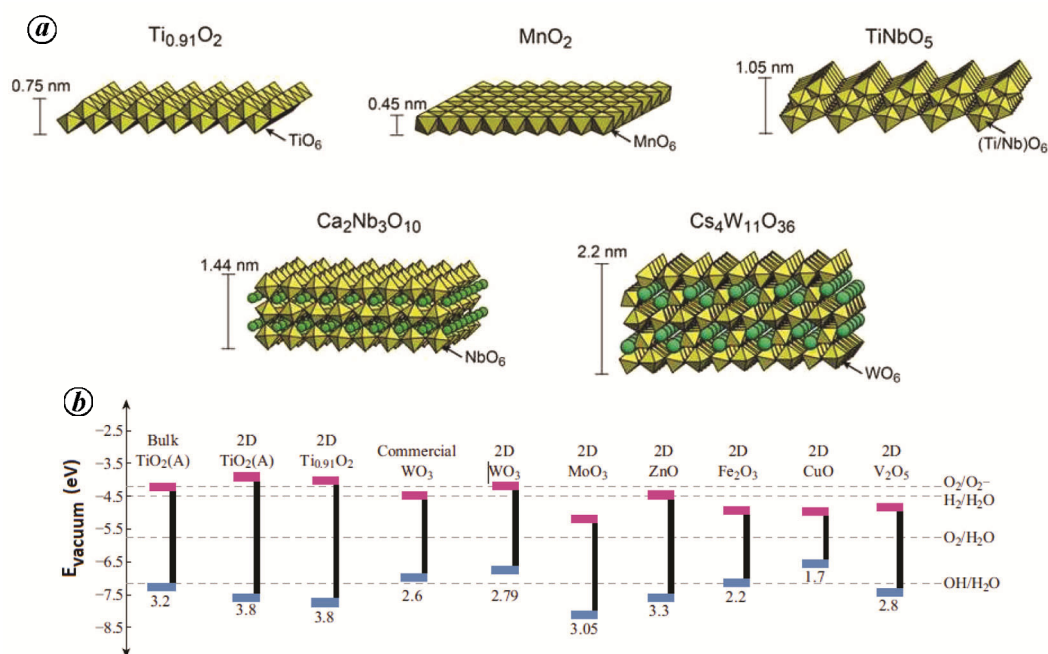


Figure 8. *a*, Structure and thickness of $\text{Ti}_{0.91}\text{O}_2$, MnO_2 , TiNbO_5 , $\text{Ca}_2\text{Nb}_3\text{O}_{10}$ and $\text{Cs}_4\text{W}_{11}\text{O}_{36}$ 2D oxides (reprinted with permission from Osada and Sasaki³¹; ©2019 by the American Physical Society). *b*, Energy band gap of various 2D transition metal oxides (reprinted from Haque *et al.*¹¹¹).

Pervoskite-type oxides like $\text{La}_{0.90}\text{Eu}_{0.05}\text{Nb}_2\text{O}_7$, $\text{K}_{1.5}\text{Eu}_{0.5}\text{Ta}_3\text{O}_{10}$, KLnNb_2O_7 , $\text{K}_2\text{Ln}_2\text{Ti}_3\text{O}_{10}$ and $\text{RbLnTa}_2\text{O}_7$ (Ln, lanthanide ion), $\text{KCa}_2\text{Nb}_3\text{O}_{10}$, $\text{Cs}_{0.7}\text{Ti}_{1.825}\text{O}_4$, $\text{K}_{0.45}\text{MnO}_2$, RbTaO_3 and $\text{Cs}_{6+x}\text{W}_{11}\text{O}_{36}$ have been exfoliated into nanosheets using chemical exfoliation methods⁶³. Figure 8a shows the structure and thickness of $\text{Ti}_{0.91}\text{O}_2$, MnO_2 , TiNbO_5 , $\text{Ca}_2\text{Nb}_3\text{O}_{10}$ and $\text{Cs}_4\text{W}_{11}\text{O}_{36}$ 2D oxides. Figure 5c shows the STM topographic image of LiTi_2O_4 thin film⁶².

Band structure and electronic properties of 2D layered oxides: The electronic properties of 2D oxides can range from being an insulator, a wide-band semiconductor to a semiconductor under different synthesizing processes and under different structures assemblies. In nanosheets, the empty d -orbital of the metal (d^0) and filled p -orbitals of the binding atom together form an insulator and wide band gap semiconductor⁶⁴. The Nb_3O_8 film formed by the deposition of consecutive films produces anodic photocurrent when the 270 nm UV light is incident on it with an efficiency (photon-to-electron) of 1.8%. UV radiotherapy results indicate the indirect wide band gap of 3.58 eV and flat band potential of 1.32 V versus Ag/Ag^+ . This is similar to $\text{Ti}_{0.91}\text{O}_2$ nanosheets in which band gap of 3.84 eV and flat band potential of 1.27 V versus Ag/Ag^+ have been observed^{65,66}. Superlattice can be artificially developed using perovskite oxide nanosheets of LaNb_2O_7 and $\text{Ca}_2\text{Nb}_3\text{O}_{10}$ (ref. 12). The superlattice formation leads to low leakage current, which is the most desirable parameter at the nanoscale level. Beyond this, the current parameters of 2D oxide nano-

sheets can also be re-engineered by A and B site modification. In $\text{Ca}_2\text{Nb}_3\text{O}_{10}$ nanosheets, lattice substitution of the A and B sites with Sr^{2+} and Ta^{5+} ions showed that the value of dielectric constant was further enhanced by 30–110 (ref. 67).

Optical properties of 2D layered oxides: The radiant property of different layered perovskites with A site substitution, having their Ln^{3+} ions substituted with $\text{Eu}^{3+}/\text{Tb}^{3+}$ ions, gave red and green emission respectively¹¹⁰. Similarly red emission was observed when $\text{Gd}_{1.4}\text{Eu}_{0.6}\text{Ti}_3\text{O}_{10}$ and $\text{La}_{0.7}\text{Tb}_{0.3}\text{Ta}_2\text{O}_7$ were excited with 254 nm wavelength⁶⁸. Optical properties of nanosheets are anisotropic and thus can be modified by changing the orientation of nanosheets in the magnetic field⁶⁸.

Magnetic properties of 2D layered oxides: Several TiO_2 nanosheets like $\text{Ti}_{0.8}\text{Co}_{0.2}\text{O}_2$ have shown ferromagnetism at room temperature⁶⁹. They exhibit highly anisotropic behaviour when intensity of magnetization is measured along the equatorial and axial lines. $\text{Ti}_{0.8}\text{Co}_{0.2}\text{O}_2$ showed the highest magnetic dipole moment of 1.4 $\mu\text{B}/\text{Co}$ when the film was parallel to the magnetic field, which was 1.5 times higher in comparison to the orthogonal direction, along with the spin moment of 1 $\mu\text{B}/\text{Co}$ for the low-spin state of Co^{2+} which stabilizes the ferromagnetic ordering⁷⁰.

Applications of 2D layered oxides: The superlattice structure in 2D oxide nanosheets forms well-structured

quantum wells. Hence it can be deployed in diode lasers and other optoelectronic devices¹². The A and B site engineering has produced structures having a large dielectric constant (of up to 110)⁶⁷. They can thus be utilized for energy storage, large capacitors and electro-chemical energy storage (EES) systems⁷¹. Several doped nanosheets such as $\text{Ti}_{0.8}\text{Co}_{0.2}\text{O}_2$, $\text{Ti}_{0.6}\text{Fe}_{0.4}\text{O}_2$ and $\text{Ti}_{0.75}\text{Fe}_{0.1}\text{Co}_{0.15}\text{O}_2$, $\text{Ti}_{(5.2-2x)/6}\text{Mn}_{x/2}\text{O}_2$ ($x = 0.0-0.4$), sodium/potassium iron oxide show ferromagnetic properties which are useful for making magnetic tapes, hard disks and other similar memory storage devices⁷⁰.

Two-dimensional Xenes

The 2D structures of silicon, tin, germanium, phosphorous and boron, i.e. silicene, stanene, germanene, phosphorene and borophene respectively, are grouped under Xenos (X refers to the metal whose 2D structure is considered). Xenos can have elemental, decorated and composite crystal structures. In the stable state, Xenos form a buckled hexagonal structure⁷². Depending upon the buckling parameter δ , which explains the separation between different atomic horizontal planes, the various Xenos can

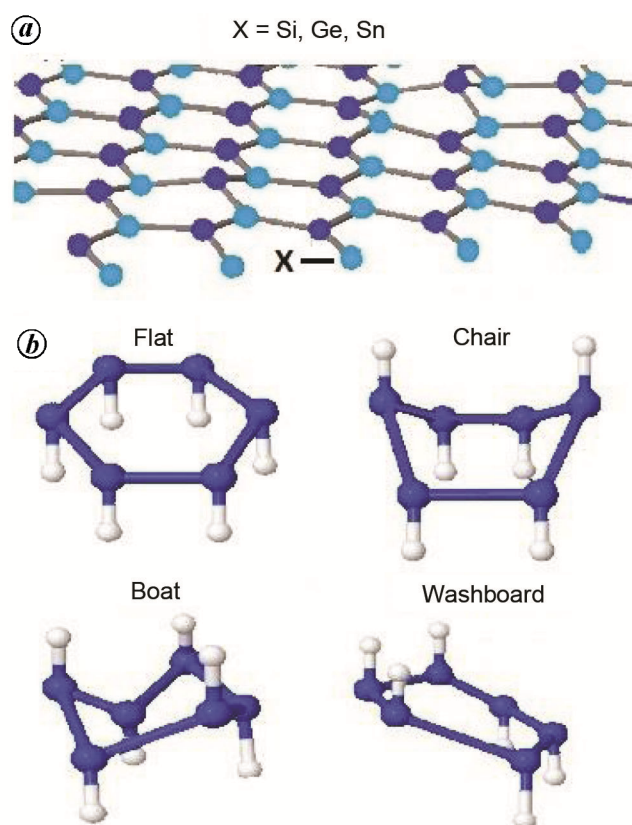


Figure 9. *a*, Bent structure of 2D nanosheets (where X = silicon, germanium and tin atoms). The dark blue coloured atoms are displaced higher in the atomic plane than the light blue coloured atoms. The distance between two horizontal planes is the buckling parameter δ . *b*, Different buckled structures, i.e. flat, chair, boat and washboard.

be differentiated according to their structure (Figure 9 *b*). Moreover, depending upon the foreign atom used and adsorption sites, different buckled structures like flat, boat, chair and washboard-type can be obtained⁷³. The boat and washboard arrangements are unstable and convert into the flat structure according to the DFT studies⁶⁴. In comparison, the chair-like structure is more stable than the flat structure⁷³. In Figure 9 *a* and *b*, silicene, germanene and stanene have been shown as a single general structure. On the other hand, phosphorene has a unique and vertically distorted hexagonal structure (Figure 10 *b*). Borophene too has different hexagonal structural phases (Figure 10 *c-e*).

Structures of 2D Xenos: Silicene, a 2D allotrope of silicon having honeycomb lattice structure, has sublattices A and B displaced comparatively in an orthogonal direction to the atomic plane, forming a small buckled structure (Figure 9 *a*). It has a buckling height of 0.44 Å and lattice constant of 0.3868 nm (ref. 74). Germanene, a 2D allotrope of germanium, has a hexagonal honeycomb structure, but with a buckling height of 0.68 Å and lattice constant 0.4060 nm (ref. 75). Due to different buckling parameters, it has different properties compared to other Xenos. Stanene, a 2D structure of tin, is a topological insulator with a band gap of 73.5 meV due to the opening of a spin-orbit gap⁷⁶. Stanene, like other Xenos, has a honeycomb lattice structure with a buckling height of 0.85 Å (ref. 77) and lattice constant of 0.4673 nm. Unlike graphene, it has weak π bonding. As a result, a low buckling structure arises from σ - π hybridization to form a stabilized 2D structure⁷⁷. Phosphorene is orthorhombic in nature⁷⁸, with a buckling height of 2.5 Å and lattice constant of 0.453 nm (refs 4 and 78). The name of phosphorene comes due to its similarity of structure with graphene⁷⁹. According to the IUPAC norms it should have been named as 2D phosphane⁷⁹. Figure 10 *a* and *b* shows ball-stick model of few layered phosphorus and puckered hexagonal structure of monolayer phosphorene. Borophene, the 2D sheet of boron, has been synthesized recently on an Ag substrate under high vacuum conditions⁸⁰. Borophene heterostructures indicate that the different layers can be stacked up due to van der Waals forces. Depending on the arrangement of the B-atoms with different periodic boron vacancy in hexagonal pattern, borophene structures can be grouped into three types (Figure 10 *c-e*)⁸¹.

Synthesis techniques of 2D Xenos: The synthesis of 2D Xenos can be done using two major methods, i.e. by segregation from bulk solids, viz. top-down approach or by bottom-up approach. PVD, CVD and micromechanical exfoliation are some of the techniques used (Figure 11)⁸². The major problem with the synthesis is that 2D Xenos are unstable in ambient temperature. Silicene synthesis was first reported by Vogt *et al.*⁸³, who observed its growth on Ag(111). Silicene has also been synthesized

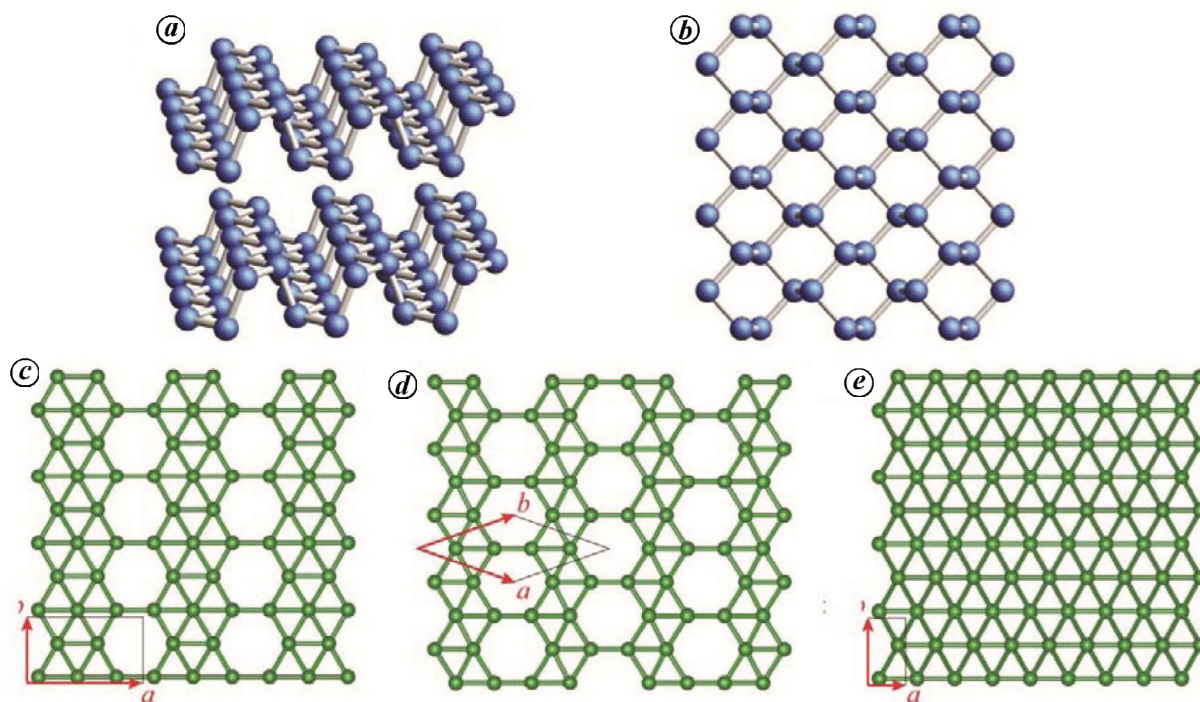


Figure 10. *a*, Ball-stick model of layered phosphorous. *b*, Puckered hexagonal structure of monolayer phosphorene (reprinted with permission from Tran *et al.*⁷⁹, ©2019 by the American Physical Society). *c-e*, β_{12} , X_3 and striped structural forms of borophene respectively (reprinted from Peng *et al.*⁸¹).

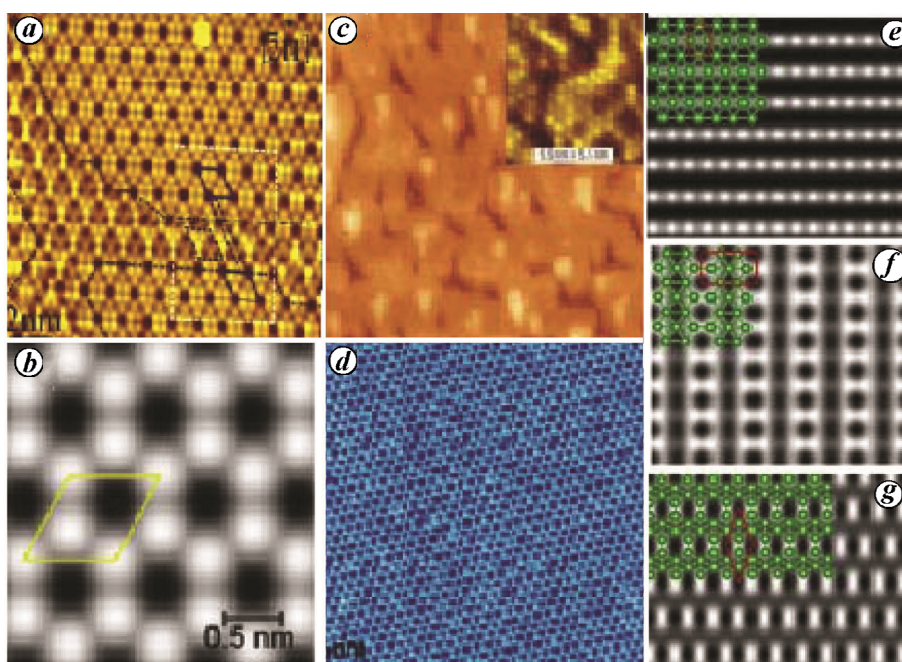


Figure 11. *a*, STM image taken on 4×4 phase domains of silicene Ag(111) (reprinted from Liu *et al.*¹¹⁶). *b*, STM image of germanene with 2×2 periodicity on Au(111) (super cells in the STM image are highlighted with yellow line) (reprinted from Dávila *et al.*¹¹⁷). *c*, STM images of stanene on Bi₂Te₃(111) (reprinted from Li *et al.*¹¹⁸). *d*, STM image of multilayer blue-phosphorene on Au(111) (reprinted from Hu *et al.*¹¹⁹). *e-g*, STM images of borophene $v_{1/5}$ sheet with overlaid atomic structure (freestanding a triangular, β_{12} , and X_3 boron sheets respectively) (reprinted from Luo *et al.*¹²⁰).

on Ir(111), MoS₂ and ZrB₂(0001) crystals⁸⁴. Germanene also shows surface-assisted growth by molecular beam epitaxy (MBE) under ultra high-vacuum (UHV) condi-

tions⁸⁴. The first surface-assisted growth of stanene was seen on Bi₂Te₃(111) crystal under UHV conditions at room temperature⁸⁵. For phosphorene, the most common

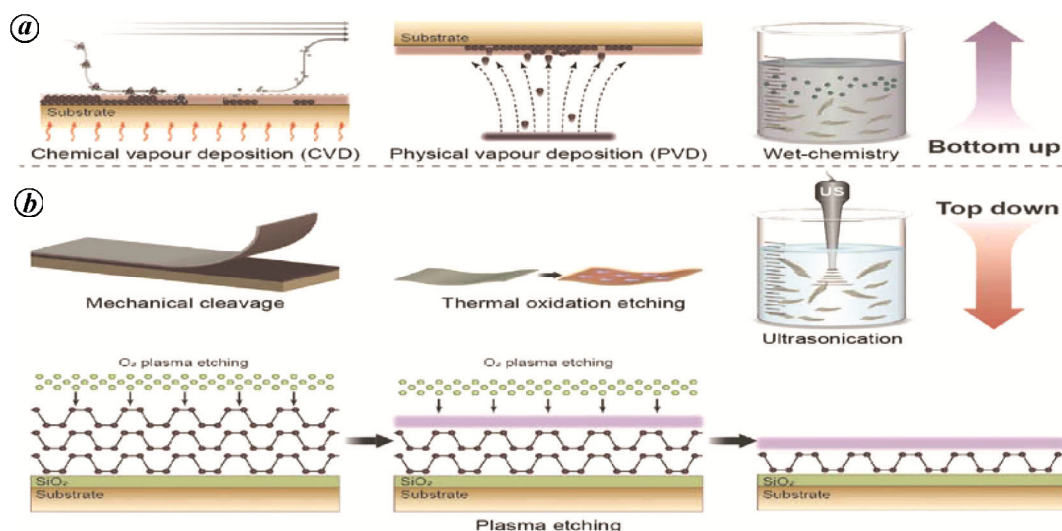


Figure 12. Different synthesis techniques for Xenes (reprinted from Tao *et al.*⁸²).

growth synthesis method is the exfoliation of black phosphorus⁸⁶. CVD is used for the synthesis of black phosphorus from its bulk form and 2D sheets are separated from it by micromechanical/solution-based exfoliation processes⁸⁶. Borophene synthesis has issues of adulterants, purity of source and compatibility with the substrate. UHV MBE helped solved the major synthesis challenges using a pure solid atomic boron source on Ag(111) substrates⁸⁷. Figure 12 shows the STM images of silicene, germanene, stanene, phosphorene and borophene.

Band structure and electronic properties of 2D Xenes: From DFT simulations, silicene is found to be a zero band gap semiconductor with sp^2 hybridization (Figure 13 a). It is found in a meta-stable buckled form due to preferred sp^3 hybridization of Si atoms⁸⁸. Band gap engineering allows the opening of a band gap in silicene by the application of an external electric field⁸⁹. Quasi particle interference (QPI) pattern reveals the presence of Dirac cone and relativistic particles having Fermi velocity of the order $1.2 \times 10^6 \text{ ms}^{-1}$ in silicene⁹⁰. The Fermi velocity in silicene is comparatively less than that in graphene due to the weak π interactions⁹⁰. The buckling structure of silicene has the least effect on its Fermi velocity. Spin-orbit coupling induces the quantum spin hall (QSH) effect due to the opening of band gap at Dirac point⁸⁹. Due to QSH there is a speedy phase transition of silicene from the semi-metallic nature to an insulator⁸⁹.

Like graphene, germanene also shows a honeycomb structure (Figure 9 a). Since it has a buckled structure, its electronic properties are different compared to graphene. The germanene monolayer is a semi-metal with zero forbidden energy band gap and Dirac cone is present at the Fermi level (Figure 13 b). The buckled structure provides the possibility of opening a band gap if a vertical electrical

field is applied⁹¹. The spin-orbit coupling interaction splits the energy band levels and introduces a band gap of around 20 meV in Germanene⁹².

Stanene, which is a QSH, has brought a new dimension in the field of nanoelectronics because of edge transport⁹³. Stanene has a 73.5 meV band gap due to spin-orbit coupling. Its value is substantially greater than the band gap of graphene, silicene and germanene (Figure 13 c)⁹³. Further, the halogenation of stanene could enlarge the band gap to 300 meV, which promotes its usage at room temperature⁹⁴. The Fermi velocity of fluorinated stanene is up to $6.8 \times 10^5 \text{ m/s}$ (ref. 94).

In phosphorene, the band structure depends upon the number of layers of nanosheets. It has its band gap in the range 0.3 eV (for bulk) to 2.0 eV (for monolayer⁸⁶) (Figure 13 e and f). As the layer count is decreased to monolayer, phosphorene shifts its nature from being an indirect to a direct band gap semiconductor. Theoretical studies suggest the process of hydrogen passivation to form direct band gap phosphorene nanoribbons which are stable⁷⁶. Further, edge termination controls its tunability⁷⁶. Different studies also report the effect of strain on electronic properties. Strain can be used to control the effective mass of an electron, its direction of mobility and induce direct to indirect transition in the energy band gap⁹⁵. A few layers of quasi 2D phosphorene display carrier mobility of up to $1000 \text{ cm}^2 \text{ V}^{-1} \text{ s}^{-1}$ at room temperature⁹⁶.

In borophene, superconductivity and topological properties are better compared to graphene⁹⁷. Its Fermi velocity is $3.6 \times 10^6 \text{ ms}^{-1}$ (almost four times that of graphene)⁹⁸. The BCS (Bardeen-Cooper-Schrieffer) theory of superconductivity states that the light-weight elements are beneficial for increasing the superconducting transition temperature (T_c), as the Debye temperature for these materials is high⁹⁹. Graphene, silicene and phosphorene

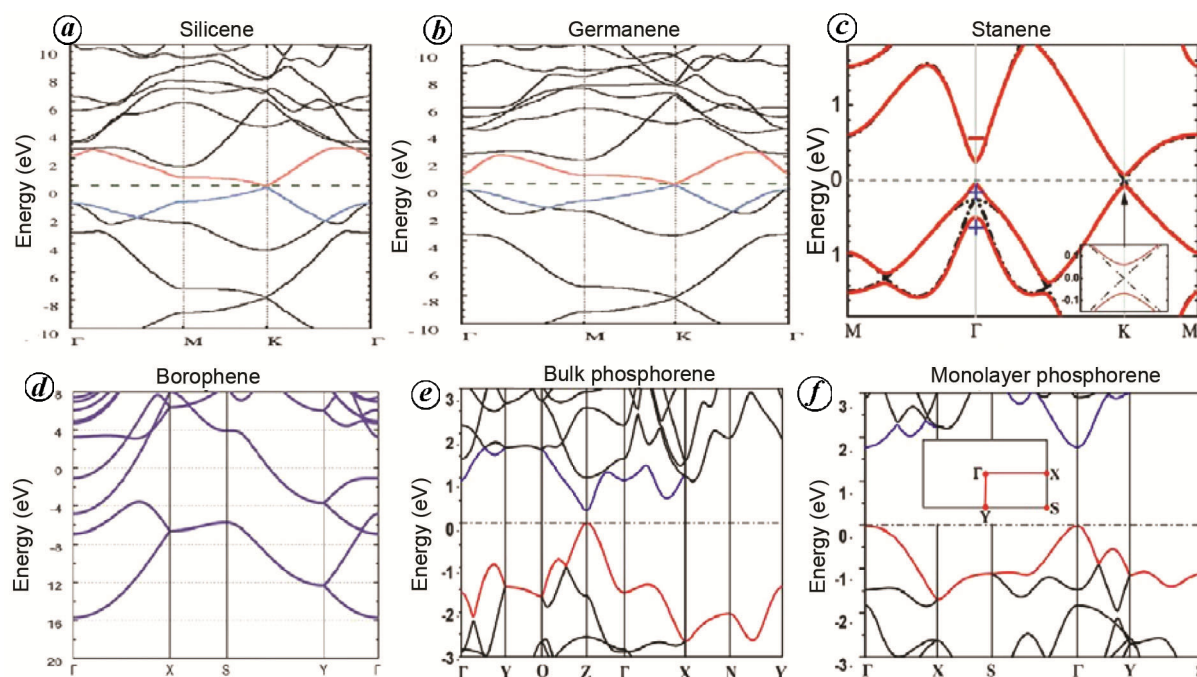


Figure 13. Band structures of (a) silicene (reprinted with permission from Miro *et al.*¹²¹), (b) germanene (reprinted with permission from Miro *et al.*¹²¹), (c) stanene (reprinted with permission from Xu *et al.*⁹⁴, ©2019 by the American Physical Society), (d) borophene (reprinted with permission from Peng *et al.*¹⁸) and (e, f) bulk and monolayer phosphorene (reprinted with permission from Lv *et al.*¹⁰⁰).

are not suitable to produce high T_c , while B atoms show strong electron–phonon coupling and thus show superconductivity⁹⁷.

Optical properties of 2D Xenos: For their applications in optoelectronics, optical properties like light absorption, emission and efficiency of photo conversion of 2D Xenos play an important role. A wide bandwidth of absorption spectra ranging from UV rays, visible light to near and far infrared spectroscopy in Xenos find applications in the biomedical field. The excellent photo-thermal conversion efficiency (about 50%) promotes usage of Xenos as photo-sensitizers, which can effectively as well as selectively kill both bacteria and cancer cells⁸². Phosphorene is observed to have a strong localized surface plasmon resonance effect, which advocates its usage as a substrate for the surface-enhanced Raman spectroscopy (SERS)¹⁰⁰. Along with their built-in biocompatibility, SERS makes Xenos promising for high-resolution imaging and Raman scattering-based sensor device applications⁸². The luminescence properties of Xenos could be used for bio-imaging and optical sensors^{82,100}. These optical properties can be optimized and tuned in by forming Xenos with different composition, size, thickness and surface modification which can be utilized in different applications¹⁰⁰.

Mechanical properties of 2D Xenos: For nanoelectromechanical systems, the mechanical properties of 2D Xenos hold high significance. In a study, the stiffness was found to be inversely proportional to the increasing atomic

weight (i.e. Si to Sn)¹⁰¹. In silicene, mechanical flexibility changes as a function of bond angle, while for graphene the C–C bond length is observed to increase as a function of axial strain¹⁰¹. This exclusive property in silicene makes it highly adaptable for use in flexible electronics. In germanene, on application of axial strain, transformation occurs from chair to washboard-like structure⁷³. The Young's modulus of silicene, germanene, stanene and phosphorene was found to be direction-dependent, with values of 61.7 and 59 GPa, 44 and 43.4 GPa, 25.2 and 23.5 GPa and 166 and 44 GPa along zigzag and armchair directions respectively¹⁰². Borophene with even 1/6 HH concentration has a bending stiffness four times lower than that of graphene and Young's modulus of about 210 N m⁻¹ which is 60% more than that of graphene¹⁰³. In addition to high in-plane elasticity of borophene, its low mass density further leads to a specific modulus of 346 m² s⁻², which is almost similar to graphene, and hence can be used in flexible electronics¹⁰³.

Magnetic properties of 2D Xenos: Magnetic properties of 2D Xenos can be transformed by using different surface substrates, chemisorption, introduction of point defects, electrostatic doping, application of external electric field and inducing periodic deformation¹⁰⁴. Silicene exhibits ferromagnetic behaviour when half hydrogenated, and anti-ferromagnetic behaviour when half brominated¹⁰⁵. In a study, magnetism was induced in transition metal-decorated Xenos. Similar behaviour to silicene was

Table 1. Summary of two-dimensional materials and their potential applications

Materials	Structural phases	Band gap (eV)	Unique electronic properties	Mechanical properties	Magnetic properties	Potential application
Transition metal dichalcogenides	Trigonal prismatic (2H) Octahedral (1T). Distorted 1T ^{19,25}	MoS ₂ (2H) bulk and monolayer 0.88 and 1.71 respectively ³²	High carrier mobility (200 cm ² V ⁻¹ s ⁻¹) High on/off ratio (10 ⁸) (ref. 33)	High Young's modulus of 270 GPa (ref. 36)	Induced ferromagnetism ¹⁰¹	Optoelectronic photodetectors Flexible electronics ⁴⁰
Hexagonal boron nitride	Honeycomb structure ¹¹	3.05–5.69 (ref. 3)	High electrical resistivity of 10 ¹⁷ Ohm-cm which can be reduced by doping ¹¹	Young's modulus 220–510 N/m (ref. 54)	Magnetic properties depend upon the functional groups attached ⁵⁶	UV emitters, quantum computing ⁶⁰ , junction tunnelling devices ⁶⁰ . Biomedical applications, gas sensors ⁴⁹
Two-dimensional layered oxide	Layered structure ⁶¹	1.8–4.8 (ref. 111)	High dielectric constant value ranging from 30 to 110 (ref. 67)	A wide range	Ferromagnetism seen in TiO ₂ nanosheets ⁶⁹	Diode, Lasers, memory-based devices ⁷⁰
Silicene	Buckled honeycomb with buckled height of 0.44 Å (ref. 74)	0.1–0.4 (ref. 89)	High Fermi velocity of 1.2 × 10 ⁶ m s ⁻¹ (ref. 90), quantum spin hall effect ⁷⁴	Young's modulus of 61.7 and 59 GPa along zigzag and armchair directions respectively ¹⁰²	Can be ferromagnetic or anti-ferromagnetic ¹⁰⁵	Quantum computing, spin electronics-based devices ^{106,117}
Germanene	Buckled honeycomb with buckled height of 0.68 Å (ref. 75)	0.1–1.6 (ref. 91)	2D topological insulator ¹⁰⁹	Young's modulus of 44 and 43.4 GPa along zigzag and armchair directions respectively ¹⁰²	Can be ferromagnetic or anti-ferromagnetic ¹⁰⁵	Spin electronics and quantum information processing ¹⁰⁸
Stanene	Buckled honeycomb with buckling height of 0.85 Å (ref. 77)	0.1–1.6 (ref. 93)	Superconductor, high Fermi velocity of the order of 6.8 × 10 ⁵ m/s (ref. 77)	Young's modulus of 25.2 and 23.5 GPa along zigzag and armchair directions respectively ¹⁰²	Can be ferromagnetic or anti-ferromagnetic ¹⁰⁵	Ultrafast FET's, wiring system, low power devices ⁹⁴
Phosphorene	Puckered hexagonal structure with buckling height of 2.5 Å (ref. 4)	0.3–2 (ref. 86)	High carrier mobility (1000 cm ² V ⁻¹ s ⁻¹) ⁷⁹	Young's modulus of 166 and 44 GPa along zigzag and armchair directions respectively ¹⁰²	Can be ferromagnetic or anti-ferromagnetic ¹⁰⁵	Photo transistors, gas sensors ^{96,100}
Borophene	B ₁₂ , X ₃ , striped ⁸¹	0.1–1.6 (ref. 112)	High Fermi velocity of 3.5 × 10 ⁶ m s ⁻¹ (4 times high than graphene) ⁹⁸	Young's modulus up to 210 N/m (60% more than graphene) ¹⁰³	Can be ferromagnetic or anti-ferromagnetic ¹⁰⁵	Flexible electronics ¹⁰³

observed in germanene and stanene, in which highest magnetism was induced by Cr adatoms adsorption¹⁰⁴.

Applications of 2D Xenos: Silicene finds applications in nano-level light-emitting diodes¹⁰⁶ and quantum computing¹⁰⁷, as it has a unique property of hopping between topological insulator and topological superconductor. In germanene, the use of spin rather than just its charge has been utilized in quantum information processing¹⁰⁸. It is also an optically active material and so could be used in optoelectronics applications¹⁰⁹. Further, its tunable band gap could be deployed in tunable nanoelectronics applications. Due to large Fermi velocity of the edge state (6.8×10^5 m/s), stanene can be considered for wiring systems that link various parts of a microprocessor⁹⁴. Due to the free flow of electrons, heat generation would be less and power consumed will also be low; this will help in the production of energy-efficient electronic devices. Few-layered black phosphorus has been integrated into photo-transistors with a good response^{96,110}. Its heterojunction with BN and MoS₂ exhibits photovoltaic effect. Further, the high binding capacity for nitrogen based gas molecules shows its use as gas sensors^{76,96}. It could be used in various superconductor applications. Borophene of $v_{1/6}$ sheet having 1/6 HH concentration exhibits bending stiffness which is four times lower than that of graphene and the Young's modulus of the $v_{1/6}$ sheet reaches up to 210 Nm⁻¹ (ref. 103). So borophene can be used in flexible electronics.

Conclusion and future scope

Owing to the superior electronic, mechanical, optical and magnetic properties, the 2D structural analogues other than graphene could eventually be adopted for a wide range of nanoelectronics applications. TMDs with 1–2 eV energy band gap and high on/off ratios could be deployed in low-power VLSI circuits. Due to their low working bias and ultra sensitivity, they have potential usage in optoelectronic circuits. h-BN behaves as a good dielectric material and graphene-based FETs show better characteristics when they use h-BN as a surface substrate. Silicene and germanene can be used in the current Si and Ge-based technology. Further the ballistic transport properties and presence of Dirac cone in silicene and germanene could help realize ultra-high speed nanoelectronics devices. Environmental robustness and high oxidation resistance of silicene and germanene are added advantages and render them desirable for various industrial and military applications. The same could be extended to the usage of stanene, but it requires further research. Phosphorene follows graphene in integration with the present-day technology. Recent advancements in the research on phosphorene show the remarkable properties of this material and inspire its rapid exploration for

usage in high-speed electronics. When compared to graphene, phosphorene is a direct band gap semiconductor, which is one of its desirable features. Because of the narrow band gap, phosphorene could be utilized in various optoelectronic devices and nano-sensors. Many of its mechanical, optical, electronic and thermal properties are yet to be standardized. Borophene shows better superconductivity compared to graphene, because of its high electron density and edge transport feature. Although 2D oxide sheets lag behind graphene in transport properties, they outperform in terms of flexibility and compressibility. These features of 2D oxide sheets find usage in flexible and spin-based electronics. Further studies are required to explore the quantum dynamics of these materials so that they can be considered for various customized applications at the nano-scale. This aspect of controlling their properties can pave a new path for low-dimensional, economical and durable nanoelectronics applications in the near future.

The lack of progress to standardize the synthesis techniques and experimental processes has limited the scope to explore various theoretical predictions beyond graphene 2D materials. So far, only substrate-assisted epitaxial growth for 2D Xenos has been reported. This limitation is because these materials are meta-stable. Alternate approaches to produce independent 2D sheets and to cleave them from their substrates are still to be explored in detail. Thus, the advancement in synthesis techniques to produce free-standing 2D alternative materials will be a significant breakthrough for utilizing the full potential of these 2D materials in the evolution of next-generation electronic, spin electronic and optoelectronic device applications. Table 1 summarizes the structural phases, band gaps, unique electronic, mechanical and magnetic properties along with potential applications for the ease of future work in the field.

1. Geim, A. K. and Novoselov, K. S., The rise of graphene. *Nature Mater.*, 2007, **6**, 183–191.
2. Chhowalla, M., Shin, H. S., Eda, G., Li, L.-J., Loh, K. P. and Zhang, H., The chemistry of two-dimensional layered transition metal dichalcogenide nanosheets. *Nature Chem.*, 2013, **5**(4), 263–275; doi:10.1038/nchem.1589.
3. Chen, W. *et al.*, Hydrogenation: a simple approach to realize semiconductor–half metal–metal transition in boron nitride nanoribbons. *J. Am. Chem. Soc.*, 2010, **132**, 1699–1705.
4. Favron, A. *et al.*, Photo oxidation and quantum confinement effects in exfoliated black phosphorus. *Nature Mater.*, 2015, **14**, 826–832.
5. Gregory, A. *et al.*, Graphene ballistic nano-rectifier with very high responsivity. *Nature Commun.*, 2016, **7**, 11670.
6. Tang, Q. and Zhou, Z., Graphene-analogous low-dimensional materials. *Prog. Mat. Sci.*, 2013, **58**, 1244–1315.
7. Jun, Y. W., Seo, J. W., Oh, S. J. and Cheon, J., Recent advances in the shape control of inorganic nano-building blocks. *Coord. Chem. Rev.*, 2005, **249**, 1766–1775.
8. Wang, K., Yin, P., Zhang, Y. and Jiang, W., Phase diagram and magnetization of a graphene nano-island structure, *Physica A*, 2018, **505**, 268–279.

9. Xin, W. *et al.*, One-step synthesis of tunable-size gold nanoplates on graphene multilayers. *Nano Lett.*, 2018, **18**, 1875–1881.
10. Banszerus, L. *et al.*, Ballistic transport exceeding 28 μm in CVD grown graphene. *Nano Lett.*, 2016, **16**, 1387–1391.
11. Lin, Y. and Connell, J. W., Advances in 2D boron nitride nanostructures: nanosheets, nanoribbons, nanomeshes, and hybrids with graphene. *Nanoscale*, 2012, **4**, 6908–6939.
12. Osada, M. and Sasaki, T., Exfoliated oxide nanosheets: new solution to nanoelectronics. *J. Mater. Chem.*, 2009, **19**, 2503–2511.
13. Jiang, Z., Zhang, Y., Tan, Y. W., Stormer, H. L. and Kim, P., Quantum hall effect in graphene, *Solid State Commun.*, 2007, **143**, 14–19.
14. Novoselov, K. S., Jiang, Z., Zhang, Y., Morozov, S. V., Stormer, H. L., Zeitler, U. and Geim, A. K., Room-temperature quantum hall effect in graphene. *Science*, 2007, **315**(5817), 1379–1379; doi:10.1126/science.1137201.
15. Chuang, H.-J. *et al.*, Low-resistance 2D/2D ohmic contacts: a universal approach to high-performance WSe₂, MoS₂ and MoSe₂ transistors. *Nano Lett.*, 2016 **16**(3), 1896–1902; doi: 10.1021/acs.nanolett.5b05066.
16. Zhu, Q., Xu, Z., Li, J. G., Li, X., Qi, Y. and Sun, X., Hydrothermal-assisted exfoliation of Y/Tb/Eu ternary layered rare-earth hydroxides into tens of micron-sized uni-lamellar nanosheets for highly oriented and color-tunable nano-phosphor films. *Nanoscale Res. Lett.*, 2015, **10**, 132.
17. Robinson, J. A., Schaak, R. E., Sun, D., Sun, Y., Mallouk, T. E. and Terrones, M., Transition metal dichalcogenides and beyond: synthesis, properties, and applications of single- and few layer nanosheets. *Acc. Chem. Res.*, 2014, **48**(1), 56–64; doi:10.1021/ar5002846.
18. Meng, L. *et al.*, Buckled silicene formation on Ir(111). *Nano Lett.*, 2013, **13**, 685–690.
19. Ozawa, T. C., Fukuda, K., Akatsuka, K., Ebina, Y. and Sasaki, T., Preparation and characterization of the Eu³⁺ doped perovskite nanosheet phosphor: La_{0.9}Eu_{0.05}Nb₂O₇. *Chem. Mater.*, 2007, **19**, 6575–6580.
20. Lalm, B., Oughaddou, H., Enriquez, H., Kara, A., Vizzini, S., Ealet, B. and Aufray, B., Epitaxial growth of a silicene sheet. *Appl. Phys. Lett.*, 2012, **97**, 223109.
21. Fleurence, A., Friedlein, R., Ozaki, T., Kawai, H., Wang, Y. and Yamada-Takamura, Y., Experimental evidence for epitaxial silicene on diboride thin films. *Phys. Rev. Lett.*, 2012, **108**, 245501.
22. Zhao, J. *et al.*, Rise of silicene: a competitive 2D material. *Prog. Mater. Sci.*, 2016, **83**, 24–151.
23. Cunningham, G. *et al.*, Solvent exfoliation of transition metal dichalcogenides: dispersibility of exfoliated nanosheets varies only weakly between compounds. *ACS Nano*, 2012, **6**, 3468–3480.
24. Hernandez, Y. *et al.*, High-yield production of graphene by liquid-phase exfoliation of graphite. *Nature Nanotechnol.*, 2008, **3**, 563–568.
25. Radisavljevic, B., Radenovic, A., Brivio, J., Giacometti, V. and Kis, A., Single-layer MoS₂ transistors. *Nature Nanotechnol.*, 2011, **6**, 147–150.
26. Hill, H. M., Rigosi, A. F., Rim, K. T., Flynn, G. W. and Heinz, T. F., Band alignment in MoS₂/WS₂ transition metal dichalcogenide heterostructures probed by scanning tunneling microscopy and spectroscopy. *Nano Lett.* 2016, **16**, 4837–4837.
27. Choi, W. *et al.*, Recent development of two-dimensional transition metal dichalcogenides and their applications *Nano-Micro Lett.*, 2018, **10**, 23.
28. Kappera, R., Voiry, D., Yalcin, S. E., Branch, B., Gupta, G., Mohite, A. D. and Chhowalla, M., Phase-engineered low-resistance contacts for ultrathin MoS₂ transistors *Nature Mater.*, 2014, **13**, 1128.
29. Guo, Y. *et al.*, Probing the dynamics of the metallic-to-semiconducting structural phase transformation in MoS₂ crystals. *Nano Lett.*, 2015, **15**, 5081.
30. Zhu, Z. Y., Cheng, Y. C. and Schwingenschlögl, U., Giant spin-orbit-induced spin splitting in two-dimensional transition-metal dichalcogenide semiconductors. *Phys. Rev. B*, 2011, **84**, 153402.
31. Osada, M. and Sasaki, T., Chemical nanomanipulation of two-dimensional nanosheets and its applications. In *Nanofabrication* (ed. Masuda, Y.), InTech, Rijeka, Croatia, 2011, pp. 153–166.
32. Radisavljevic, B., Whitwick, M. B. and Kis, A., Correction to integrated circuits and logic operations based on single-layer MoS₂. *ACS Nano*, 2013, **7**, 3729.
33. Splendiani, A. *et al.*, Emerging photoluminescence in monolayer MoS₂. *Nano Lett.*, 2010, **10**, 1271–1275.
34. Ahmad, S. and Mukherjee, S., A comparative study of electronic properties of bulk MoS₂ and its monolayer using DFT technique: application of mechanical strain on MoS₂ monolayer. *Graphene*, 2014, **3**(4), 52–59.
35. Zeng, H., Dai, J., Yao, W., Xiao, D. and Cui, X., Valley polarization in MoS₂ monolayers by optical pumping. *Nature Nanotechnol.*, 2012, **7**, 494–498; doi:10.1038/nnano.2012.95.
36. Bertolazzi, S., Brivio, J. and Kis, A., Stretching and breaking of ultrathin MoS₂. *ACS Nano*, 2011, **5**, 9703–9709.
37. Kaplan-Ashiri, I., Cohen, S. R., Gartsman, K., Rosentsveig, R., Seifert, G. and Tennea, R., Mechanical behavior of individual WS₂ nanotubes. *J. Mater. Res.*, 2004, **19**, 454–459.
38. Cai, L. *et al.* Vacancy-induced ferromagnetism of MoS₂ nanosheets. *J. Am. Chem. Soc.*, 2015, **137**, 2622–2627.
39. Wang, H., Zhao, Y., Xie, Y., Ma, X. and Zhang, X., Recent progress in synthesis of two-dimensional hexagonal boron nitride. *J. Semicond.*, 2017, **38**, 031003.
40. Krasheninnikov, A. and Nordlund, K., Ion and electron irradiation-induced effects in nanostructured materials. *J. Appl. Phys.*, 2010, **107**, 071301.
41. Mahvash, F. *et al.*, Corrosion resistance of monolayer hexagonal boron nitride on copper. *Sci. Rep.*, 2017, **7**, 42139.
42. Wang, J., Ma, F. and Sun, M., Graphene, hexagonal boron nitride, and their heterostructures: properties and applications. *RSC Adv.*, 2017, **7**, 16801.
43. Wiechert, H., Adsorption of molecular hydrogen isotopes on graphite and BN. In *Absorbed Layers on Surfaces* (ed. Bonzel, A. P.), Springer, 2003, pp. 166–196.
44. Zeng, H. *et al.*, ‘White graphenes’: boron nitride nanoribbons via boron nitride nanotube unwrapping. *Nano Lett.*, 2010, **10**, 5049–5055.
45. Zhi, C., Bando, Y., Tang, C., Kuwahara, H. and Golberg, D., Large-scale fabrication of boron nitride nanosheets and their utilization in polymeric composites with improved thermal and mechanical properties. *Adv. Mater.*, 2009, **21**, 2889–2893.
46. Lin, Y., Williams, T. V. and Connell, J. W., Soluble, exfoliated hexagonal boron nitride nanosheets. *J. Phys. Chem. Lett.*, 2009, **1**, 277–283.
47. Lin, Y. and Connell, J. W., Advances in 2D boron nitride nanostructures: nanosheets, nanoribbons, nanomeshes, and hybrids with graphene. *Nanoscale*, 2012, **4**, 6908–6939.
48. Liu, D. *et al.*, Conformal hexagonal-boron nitride dielectric interface for tungsten diselenide devices with improved mobility and thermal dissipation. *Nature Commun.*, 2019, **10**, 1188; <https://doi.org/10.1038/s41467-019-09016-0>.
49. Aldabahi, A. and Feng, P., Development of 2-D boron nitride nanosheets UV photoconductive detectors. *IEEE Trans. Electron. Devices*, 2015, **62**(6), 1885–1890; doi:10.1109/ted.2015.2423253.
50. Wang, V., Liu, R.-J., He, H.-P., Yang, C.-M. and Ma, L., Hybrid functional with semi-empirical van der Waals study of native defects in hexagonal BN. *Solid State Commun.*, 2014, **177**, 74–79.

51. Zhang, K., Feng, Y., Wang, F., Yang, Z. and Wang, J., Two dimensional hexagonal boron nitride (2D-hBN): synthesis, properties and applications. *J. Mater. Chem. C*, 2017, **5**(46), 1992–12022.
52. Mukherjee, S and Thilagar, P., Borophene a new paradigm. *Curr. Sci.*, 2016, **111**(8), 1302–1304.
53. Sahin, H. *et al.*, Monolayer honeycomb structures of group-IV elements and III–V binary compounds: first-principles calculations. *Phys. Rev. B*, 2009, **80**, 155453.
54. Meng, W., Huang, Y., Fu, Y., Wang, Z. and Zhi, C., Polymer composites of boron nitride nanotubes and nanosheets. *J. Mater. Chem. C*, 2014, **2**(47), 10049–10061; doi:10.1039/c4tc01998a.
55. Lee, C. *et al.*, Frictional characteristics of atomically thin sheets. *Science*, 2010, **328**, 76–80.
56. Zhou, J., Wang, Q., Sun, Q. and Jena, P., Electronic and magnetic properties of a BN sheet decorated with hydrogen and fluorine. *Phys. Rev. B*, 2010, **81**(8), 085442.
57. Lin, Y., Williams, T. V. and Connell, J. W., Soluble, exfoliated hexagonal boron nitride nanosheets. *J. Phys. Chem. Lett.*, 2009, **1**, 277–283.
58. Golberg, D. *et al.*, Boron nitride nanotubes and nanosheets. *ACS Nano*, 2010, **4**, 2979–2993.
59. Britnell, L., Gorbachev, R. V. and Jalil, R., Atomically thin boron nitride: a tunneling barrier for graphene devices. *Nano Lett.*, 2012, **12**(3), 1707–1710.
60. Chandni, U., Watanabe, K., Taniguchi, T. and Eisenstein, J. P., Evidence for defect-mediated tunneling in hexagonal boron nitride-based junctions. *Nano Lett.*, 2015, **15**(11), 7329–7333.
61. O’Leary, S., O’Hare, D. and Seeley, G., Delamination of layered double hydroxides in polar monomers: new LDH-acrylate nanocomposites. *Chem. Commun.*, 2002, 1506–1507.
62. Okada, Y. *et al.*, Scanning tunnelling spectroscopy of superconductivity on surfaces of LiTi₂O₄(111) thin films. *Nature Commun.*, **8**, 15975.
63. Geng, F. *et al.*, New layered rare-earth hydroxides with anion-exchange properties. *Chem.-Eur. J.*, 2008, **14**, 9255–9260.
64. Taniguchi, T. *et al.*, Enhanced and engineered *d*₀ ferromagnetism in molecularly-thin zinc oxide nanosheets. *Adv. Funct. Mater.*, 2013, **23**, 3140–3145.
65. Sakai, N., Ebina, Y., Takada, K. and Sasaki, T., Electronic band structure of titania semiconductor nanosheets revealed by electrochemical and photoelectrochemical studies. *J. Am. Chem. Soc.*, 2004, **126**(18), 5851–5858; doi:10.1021/ja0394582.
66. Akatsuka, K., Takanashi, G., Ebina, Y., Sakai, N., Haga, M.-A. and Sasaki, T., Electrochemical and photoelectrochemical study on exfoliated Nb₃O₈ nanosheet. *J. Phys. Chem. Solids*, 2008, **69**, 1288–1291.
67. Li, B.-W. *et al.*, Engineered interfaces of artificial perovskite oxide superlattices via nanosheet deposition process. *ACS Nano*, 2010, **4**, 6673–6680.
68. Ida, S. *et al.*, Preparation of a blue luminescent nanosheet derived from layered perovskite Bi₂SrTa₂O₉. *J. Am. Chem. Soc.*, 2007, **129**, 8956–8957.
69. Osada, M. *et al.*, Ferromagnetism in two-dimensional Ti_{0.8}Co_{0.2}O₂ nanosheets. *Phys. Rev. B*, 2006, **73**, 153301.
70. Osada, M., Ebina, Y., Takada, K. and Sasaki, T., Gigantic magneto-optical effects in multilayer assemblies of two-dimensional titania nanosheets. *Adv. Mater.*, 2006, **18**, 295–299.
71. Mahmood, N., De Castro, I. A., Pramoda, K., Khoshmanesh, K., Bhargava, S. K. and Kalantar-Zadeh, K., Atomically thin two-dimensional metal oxide nanosheets and their heterostructures for energy storage. *Energy Storage Mater.*, 2018, **16**, 455–480; doi: 10.1016/j.ensm.2018.10.013.
72. Ding, Y. and Wang, Y. L., Density functional theory study of the silicene-like SiX and XSi₃ (X = B, C, N, Al, P) honeycomb lattices: the various buckled structures and versatile electronic properties. *J. Phys. Chem. C*, 2013, **117**, 18266.
73. Matthes, L., Pulci, O. and Bechstedt, F., Massive Dirac quasi particles in the optical absorbance of graphene, silicene, germanene, and tinene. *J. Phys. Condens. Matter*, 2013, **25**, 395305.
74. Cahangirov, S., Topsakal, M., Akturk, E., Sahin, H. and Ciraci, S., Two- and one-dimensional honeycomb structures of silicon and germanium. *Phys. Rev. Lett.*, 2009, **102**, 236804.
75. Chen, H. D. and Lin, D. S., Ordered 2D structure formed upon the molecular beam epitaxy growth of Ge on the silicene/Ag(111) surface. *ACS Omega*, 2016, **1**, 357–362.
76. Qiao, J., Kong, X., Hu, Z.-X., Yang, F. and Ji, W., High mobility transport anisotropy and linear dichroism in few-layer black phosphorus. *Nature Commun.*, 2014, **5**, 4475.
77. Liao, M. *et al.*, Superconductivity in few-layer stanene. *Nature Phys.*, 2018, **14**, 344–348.
78. Liu, H., Neil, A. T., Zhu, Z., Xu, X. and Tomanek, D., Phosphorene: an unexplored 2D semiconductor with a high hole mobility. *ACS Nano*, 2014, **8**, 4033–4041.
79. Tran, V., Soklaski, R., Liang, Y. and Yang, L., Layer controlled band gap and anisotropic excitons in fewlayer black phosphorus. *Phys. Rev. B*, 2014, **89**, 235319.
80. Li, W. *et al.*, Experimental realization of honeycomb borophene. *Sci. Bull.*, 2018, **63**, 282–286.
81. Peng, B. *et al.*, Stability and strength of atomically thin borophene from first principles calculations. *Mater. Res. Lett.*, 2017, **5**, 399–407.
82. Tao, W. *et al.*, Emerging two-dimensional monoelemental materials (Xenes) for biomedical applications. *Chem. Soc. Rev.*, 2019, **48**, 2891.
83. Vogt, P. *et al.*, Silicene: compelling experimental evidence for graphene like two-dimensional silicon. *Phys. Rev. Lett.*, 2012, **108**, 155501.
84. Mannix, A. J., Kiraly, B., Hersam, M. C. and Guisinger, N. P., Synthesis and chemistry of elemental 2D materials. *Nature Rev. Chem.*, 2017, **1**(2), 0014; doi:10.1038/s41570-016-0014.
85. Zhu, F.-F. *et al.*, Epitaxial growth of two-dimensional stanene. *Nature Mater.*, 2015, **14**, 1020–1025.
86. Ramasubramanian, A. and Muniz, A. R., *Ab initio* studies of thermodynamic and electronic properties of phosphorene nanoribbons. *Phys. Rev. B*, 2014, **90**, 085424.
87. Mannix, A. J. *et al.*, Synthesis of borophenes: anisotropic, two-dimensional boron polymorphs. *Science*, 2015, **350**, 1513–1516.
88. Chen, L. *et al.*, Evidence for Dirac fermions in a honeycomb lattice based on silicon. *Phys. Rev. Lett.*, 2012, **109**, 056804.
89. Sivek, J., Şahin, H., Partoens, B. and Peeters, F. M., Adsorption and absorption of boron, nitrogen, aluminium and phosphorus on silicene: stability, electronic and phonon properties. *Phys. Rev. B*, 2013, **87**, 085444.
90. Arafune, R., Lin, C. L., Nagao, R., Kawai, M. and Takagi, N., Evidence for Dirac fermions in a honeycomb lattice based on silicon. *Phys. Rev. Lett.*, 2013, **110**(22), 229701.
91. Acun, A. *et al.*, Germanene: the germanium analogue of graphene. *J. Phys.: Condens. Matter*, 2015, **27**, 443002.
92. Chen, X., Yang, Q., Meng, R., Jiang, J., Liang, Q., Tan, C. and Sun, X., The electronic and optical properties of novel Germanene and antimonene heterostructure. *J. Mater. Chem. C*, 2016, **4**, 5434–5441.
93. Nagarajan, V. and Chandiramouli, R., Investigation of electronic properties and spin–orbit coupling effects on passivated stanene nanosheet: a first-principles study. *Superlattices Microstruct.*, 2017, **107**, 118–126.
94. Xu, Y. *et al.*, Large-gap quantum spin Hall insulators in tin film. *Phys. Rev. Lett.*, 2013, **111**, 136804.
95. Sa, B. and Li, Y. L., Strain engineering for phosphorene: the potential application as a photocatalyst. *Phys. Chem. C*, 2014, **118**(46), 26560–26568.

96. Youngblood, N., Chen, C., Koester, S. J. and Li, M., Waveguide-integrated black phosphorus photodetector with high responsivity and low dark current. *Nature Photonics*, 2015, **9**, 247–252.
97. Li, G., Zhao, Y., Zeng, S., Zulfıqar, M. and Ni, J., Strain effect on the superconductivity in borophenes. *J. Phys. Chem. C*, 2018, **122**, 16916–16924.
98. Xu, L.-C., Du, A. and Kou, L., Hydrogenated borophene as a stable two-dimensional Dirac material with an ultrahigh Fermi velocity. *Phys. Chem. Chem. Phys.*, 2016, **18**(39), 27284–27289.
99. Li, D. *et al.*, Review of thermal transport and electronic properties of borophene. *Chin. Phys. B*, 2018, **27**(3), 036303.
100. Tao, W., Kong, N. and Ji, X., Emerging two-dimensional mono-elemental materials (Xenes) for biomedical applications. *Chem. Soc. Rev.*, 2019, **48**, 2891–2912.
101. Kaltsas, D., Tsatsoulis, T., Ziogos, O. G. and Tsetseris, L., Response of silicene and germanene to uni-axial compression: superstructures, polymorph nano-ribbons, and extreme bending. *J. Chem. Phys.*, 2013, **139**(12), 124709; doi:10.1063/1.4822263.
102. Mortazavi, B., Rahaman, O., Makaremi, M., Dianat, A., Cuniberti, G. and Rabczuk, T., First-principles investigation of mechanical properties of silicene, germanene and stanene. *Physica E*, 2017, **87**, 228–232; doi:10.1016/j.physe.2016.10.047.
103. Zhang, Z., Yang, Y., Penev, E. S. and Yakobson, B. I., Elasticity, flexibility, and ideal strength of borophenes. *Adv. Funct. Mater.*, 2017, **27**(9), 1605059; doi:10.1002/adfm.201605059.
104. Krawiec, M., Functionalization of group-14 two-dimensional materials. *J. Phys.: Condens. Matter*, 2018, **30**(23), 233003; doi:10.1088/1361-648x/aac149.
105. Zheng, F.-B. and Zhang, C.-W., The electronic and magnetic properties of functionalized silicene: a first-principles study. *Nanoscale Res. Lett.*, 2012, **7**, 422.
106. Huang, B. *et al.*, Exceptional optoelectronic properties of hydrogenated bilayer silicene. *Phys. Rev. X*, 2014, **4**, 021029.
107. Lü, X. L., Xie, Y. and Xie, H., Topological and magnetic phase transition in silicene-like zigzag nanoribbons. *New J. Phys.*, 2018, **20**, 043054.
108. Herath, T. M. and Apalkov, V., Energy spectra and optical transitions in germanene quantum dots. *J. Phys.: Condens. Matter*, 2016, **28**(16).
109. Jomehpour Z. S., Roknabadi, M. R., Morshedloo, T. and Modarresi, M., Electronic and thermal properties of germanene and stanene by first-principles calculations. *Superlattices Microstruct.*, 2016, **91**.
110. Lv, H. Y., Lu, W. J., Shao, D.-F. and Sun, Y. P., Large thermoelectric power factors in black phosphorus and phosphorene, 2014; arXiv:1404.5171 [cond-mat.mtrl-sci].
111. Haque, F., Daeneke, T., Kalantar, Z. K., Ou, J. Z., Two-dimensional transition metal oxide and chalcogenide-based photocatalysts. *Nano-Micro Lett.*, 2018, **10**, 23.
112. Peng, B. *et al.*, The electronic, optical, and thermodynamic properties of borophene from first-principles calculations, *J. Mater. Chem. C*, 2016, **4**(16), 3592–3598.
113. Ni, Z. *et al.*, Tunable bandgap in silicene and germanene. *Nano Lett.*, 2012, **12**(1), 113–118.
114. Kastl, C., Chen, C. T., Koch, R. J., Schuler, B., Kuykendall, T. R., Bostwick, A. and Weber-Bargioni, A., Multimodal spectromicroscopy of monolayer WS₂ enabled by ultra-clean van der Waals epitaxy. *2D Mater.*, **5**, 045010.
115. Kim, H. D., Geometric and electronic structures of monolayer hexagonal boron nitride with multivacancy. *Nano Converg.*, 2017, **13**; doi.org/10.1186/s40580-017-0107-0.
116. Liu, Z.-L. *et al.*, Various atomic structures of monolayer silicene fabricated on Ag(111), *New J. Phys.* **16**, 2014, 075006.
117. Dávila, M. E. *et al.*, Germanene: a novel two-dimensional germanium allotrope akin to graphene and silicene. *New J. Phys.*, 2014, **16**, 095002.
118. Li, G. *et al.*, Epitaxial growth and physical properties of 2D materials beyond graphene: from monatomic materials to binary compounds. *Chem. Soc. Rev.*, 2018, **47**, 6073.
119. Hu, Z. *et al.*, Two-dimensional black phosphorus: its fabrication, functionalization and applications. *Nanoscale*, 2018, **10**, 21575–21603.
120. Luo, Z., Fan, X. and An, Y., First-principles study on the stability and STM image of borophene. *Nanoscale Res. Lett.*, 2017, **12**, 514.
121. Miro, P., Audiffred, M. and Heine, T., An atlas of two dimensional materials. *Chem. Soc. Rev.*, 2014, **43**(18), 6537–6554.

Received 18 February 2019; revised accepted 20 February 2020

doi: 10.18520/cs/v118/i11/1656-1671